Quantum synchronization and quantum state sharing in an irregular complex network

Wenlin Li, Chong Li, and Heshan Song*

School of Physics and Optoelectronic Engineering, Dalian University of Technology, Dalian 116024, China

(Received 8 July 2016; revised manuscript received 8 October 2016; published 6 February 2017)

We investigate the quantum synchronization phenomenon of the complex network constituted by coupled optomechanical systems and prove that the unknown identical quantum states can be shared or distributed in the quantum network even though the topology is varying. Considering a channel constructed by quantum correlation, we show that quantum synchronization can sustain and maintain high levels in Markovian dissipation for a long time. We also analyze the state-sharing process between two typical complex networks, and the results predict that linked nodes can be directly synchronized, but the whole network will be synchronized only if some specific synchronization conditions are satisfied. Furthermore, we give the synchronization conditions analytically through analyzing network dynamics. This proposal paves the way for studying multi-interaction synchronization and achieving effective quantum information processing in a complex network.

DOI: 10.1103/PhysRevE.95.022204

I. INTRODUCTION

Synchronization is one of the most intriguing and valuable phenomena in classical physics, and its history can be traced back to the observation of two pendulum clocks by Huygens in the 17th century [1]. In the last decade, the synchronization idea has been widely applied in the fields of control and communication [2–5], which urges people to search for similar phenomena in quantum regimes. Among them, pioneering and significant progress by Mari *et al.* [6] extended the concept of complete synchronization into a continuous variable (CV) quantum system and characterized it by a quantitative measure. Up to now, extensive attention has been paid to quantum synchronization in many physical systems [7–14], but few works have proposed it as a tool in view of applications. Recently, some effective attempts have been presented to apply quantum synchronization in signal transmission [15], parameter identification [16], and atomic clocks [8,17]. Owing to Heisenberg uncertainty [18], however, the quantum effect appears to take place as just a negative influence on synchronization behavior due to quantum fluctuation. The majority of previous works considered such a kind of synchronization of only an expectation value in quantum system, and the quantum fluctuation is neglected or regarded as a disturbance in their schemes [8,15–17].

Intuitively, an appropriate application of quantum synchronization is to provide an effective quantum correlation for quantum information processing (QIP) [19]. Different from the applications of synchronization in other fields, quantum characteristics play the important role in QIP. That is not just because synchronization means two systems take on homology evolutions, which indicates the information encryption and transmission between such two systems are convenient [20,21]. Simultaneously, a nonlocal quantum effect is indispensable in this process in order to obtain the particular security and efficiency of QIP.

Other significant advantages of quantum synchronization are controllability and accessible extendibility. Especially in recent years, it is expected that QIP can be extended well into an n-body scheme or a quantum network [22–25]. However, the crossover between the quantum synchronization and complex network remains largely unexplored. In the past decade, quantum network protocols have been based mainly on one-dimensional arrays or some regular networks in order to simplify or avoid the complex multi-interaction [26–28]. Although the synchronization and correlation in a random network constituted by some simple physical systems (identical van der Pol oscillators, for example) have been discussed in few recent works [29,30], it still remains difficult for two reasons to establish a general quantum network by applying existing results. On the one hand, processing quantum information needs more complex hybrid systems with higher dimensions and different (random) parameters (initial states). On the other hand, network theory has proved that some typical network structures can give more accurate descriptions of an actual information-processing network compared to a completely random structure [31–34].

The aim of our work is to address the above problems through proposing a QIP scheme based on the application of quantum synchronization and expanding QIP well in a complex quantum network. Specifically in this paper, we study a quantum state-sharing scheme (also called a state distribution scheme) in the frame of optomechanical systems. It is known that such a QIP process requires a genuine quantum synchronization channel since the shared quantum states need to couple with the channel directly. The synchronization channel is composed of oscillators which are twofold controlled by phonon and circuit couplings for eliminating the difference between the initial state and the dynamics parameter of each oscillator. This design allows us to obtain quantum synchronization between two completely different oscillators even in the weak coupling range; however, the system accessing the network illegally will not be synchronized with other systems because of the notable differences.

Through further discussion of network theory, we determine that the quantum synchronization can also exist in two kinds of irregular networks. The given synchronization conditions ensure that the quantum synchronization and the state sharing will always be effective even though the network topology varies with time. Because of this, we think this scheme can be well applied in actual communication processes.

*hssong@dlut.edu.cn

This paper is organized as follows: In Sec. II we introduce the definition and the properties, especially the method of measurement, of quantum synchronization. In Sec. III we analyze the dynamic of a hybrid electro-optomechanical system. We show that such a kind of system can be used as a carrier of point-to point-synchronization in Sec. IV, and this conclusion is extended to two kinds of representative networks. Finally, a summary is given in Sec. VI.

II. QUANTUM SYNCHRONIZATION THEORY IN THE HEISENBERG PICTURE

We consider two coupled quantum systems which can be completely described by the quadrature operators (e.g., dimensionless position operator $\hat{q}$ and momentum operator $\hat{p}$) in the Heisenberg picture. The difference between two systems can be characterized by the following defined error operators:

$$\hat{q}_-(t) \equiv [\hat{q}_1(t) - \hat{q}_2(t)]/\sqrt{2},$$
$$\hat{p}_-(t) \equiv [\hat{p}_1(t) - \hat{p}_2(t)]/\sqrt{2}, \tag{1}$$

and quantum complete synchronization will be realized when q_- and p_- vanish asymptotically with evolution. For further quantitative statement, we introduce a synchronization measure proposed by Mari *et al.* [6,35]:

$$S_c(t) = \langle \hat{q}_-(t)^2 + \hat{p}_-(t)^2 \rangle^{-1}. \tag{2}$$

Compared to previous works, S_c is a good metric for genuine quantum synchronization because the influence of quantum fluctuation and nonlocal quantity are both considered in this synchronization measure, meaning that it can effectively distinguish the classical synchronization (even in quantum system) and genuine quantum synchronization.

For mesoscopic CV systems, S_c can be modified as

$$S_c'(t) = \langle \delta\hat{q}_-(t)^2 + \delta\hat{p}_-(t)^2 \rangle^{-1} \tag{3}$$

by mean-field approximation. Every operator here can be rewritten as a sum of its expectation value and a small fluctuation near the expectation value; i.e., it is redefined in the following form: $\hat{o}_- = \langle \hat{o}_- \rangle + \delta\hat{o}_-$ with $o \in \{q, p\}$. Because we ignore only the expectation value of each operator in Eq. (3), S_c' contains all the quantum properties of S_c, and it can also be regarded as a quantum synchronization measure when $\lim_{t\to\infty}\langle \hat{o}_- \rangle = 0$, which is an exact classical synchronization condition. Mathematically, this is because S_c' will be equal to S_c when $\lim_{t\to\infty}\langle \hat{o}_- \rangle = 0$, and, physically, synchronization at the level of the expectation value can be regarded as a necessary condition of quantum synchronization. $S_c'(t)$ is defined as second-order quantum synchronization measure in the following discussion to reflect quantum property differences between systems, and the only source of disturbance bounding $S_c'(t)$ will be quantum (or thermal) fluctuation. Correspondingly, $\langle \hat{o}_- \rangle$ is regarded as a first-order measure to judge whether systematic synchronization error due to slightly different average trajectories is synchronous or not.

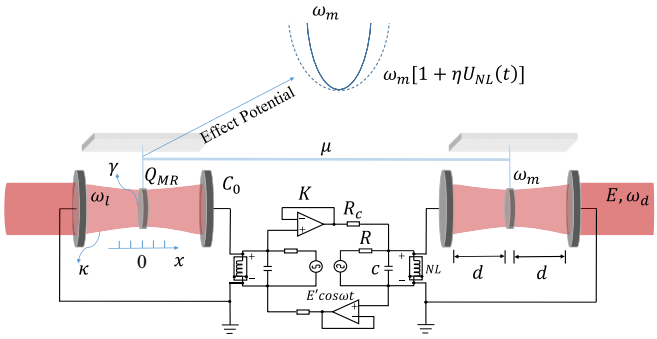

FIG. 1. Two hybrid electro-optomechanical systems are coupled via a phonon tunneling and a linear resistor. For each subsystem, a charged oscillator is placed at wave node of a Fabry-Pérot cavity, and it couples with the cavity field via a linear optomechanical interaction. An electric potential difference exists between walls of a cavity which is provided by the inductance of the Duffing circuit.

III. DYNAMICS OF A HYBRID ELECTRO-OPTOMECHANICAL SYSTEM

Let us start by focusing on the dynamics of hybrid electro-optomechanical system. As schematically shown in Fig. 1, the charged mechanical oscillators couple to the optical field and parametrically interact with the charged cavities which also play the role of electrodes. Two oscillators mutually couple through a phonon tunneling, and the electrode voltages are provided by two Duffing circuits coupled to each other via a linear resistor. We emphasize the electro-oscillator interaction is a parametric coupling because it can be thought of as a deviation in respective potential terms of two oscillators. This effect can be regarded as a time-dependent rescaling of the mirror frequency [36–41]. For a freely moving oscillator corresponding to Hamiltonian $H_m = \hat{P}^2/2m + m\omega_m^2\hat{x}^2/2$, the modified Hamiltonian under the control of the bias gate becomes

$$H_m = \frac{\hat{P}^2}{2m} + \frac{1}{2}m\omega_{\text{eff}}^2\hat{x}^2, \tag{4}$$

where $\hat{x}$ and $\hat{P}$ are the position and momentum operators of the oscillator with the bare eigenfrequency ω_m and the effective mass m. The effective frequency can be expressed as $\omega_{\text{eff}}^2 = \omega_m^2[1 + \eta U_{NL}(t)]$, where $U_{NL}(t)$ is the voltage of nonlinear inductor and η is a constant factor depending on parameters of circuit. By defining the nondimensional coordinate and momentum operators $\hat{q} = \sqrt{m\omega_m}\hat{x}$ and $\hat{p} = \hat{P}/\sqrt{m\omega_m}$ and using relation $b = (\hat{q} + i\,\hat{p})/\sqrt{2}$, Eq. (4) can be rewritten as

$$H_m = \omega_m b^\dagger b + \frac{\omega_m}{4}\eta U_{NL}(t)(b^\dagger + b)^2, \tag{5}$$

where b is phonon annihilation operator satisfying $[b, b^\dagger] = 1$. Under the modified potential, the Hamiltonian corresponding to this model can be divided into three parts:

$$H = \sum_{j=1,2} H_{0j} + H_{\text{int}} + H_{ej}, \tag{6}$$

where $H_{0j} = \omega_{lj}a_j^\dagger a_j + \omega_{mj}b_j^\dagger b_j - g a_j^\dagger a_j(b_j^\dagger + b_j) + iE(a_j^\dagger e^{-i\omega_{dj}t} - a_j e^{i\omega_{dj}t})$ is the standard Hamiltonian of the

optomechanical system [42,43], and $H_{\rm int} = -\mu(b_1^\dagger b_2 + b_2^\dagger b_1)$ is the phonon interaction through the tunneling with intensity μ [6,15]. Such an oscillator interaction can also be easily achieved by resonance oscillators with an X-X type interaction between them. After a rotating-wave approximation, X-X interaction will become $H_{\rm int}$ under the resonance condition. H_e describes the Coulomb interaction caused by two electrodes, and we will detail its expression in the following discussion.

Now we provide the details behind Eq. (5) by analyzing the dynamics of the electrical circuit system. A simple Duffing circuit can be described by the following dynamic equation [44]:

$$\frac{d^2\phi}{d\tau^2} + \frac{1}{RC}\frac{d\phi}{d\tau} + \frac{\chi_1}{C}\phi + \frac{\chi_3}{C}\phi^3 = \frac{E'}{RC}\cos\omega t. \quad (7)$$

Here χ_1 and χ_3 are constants depending on the type of the inductor, and they satisfy the relationship $i = i_R - i_C = \chi_1\phi + \chi_3\phi^3$. ϕ is the flux over the inductor; moreover, $i_R(i_L)$ and $V_R(V_L)$ are the current and voltage of the resistor (inductor), respectively. Here we make a dimensionless transformation by setting $\varphi = \phi/\phi_0, t = \tau\sqrt{\chi_1/c}, U_{NL} = d\varphi/dt, \upsilon = \phi_0^2\chi_3/\chi_1$, $\varepsilon = (R\sqrt{\chi_1 C})^{-1}, \mathbb{E} = E'/\chi_1 R\phi_0$, and $\omega_0 = \omega\sqrt{C/\chi_1}$. In this picture, the unidirectional coupling via a linear resistor can be described as a control term $\varepsilon K(U_{NL}^{\rm con} - U_{NL}^{\rm self})$, where K is coupling intensity. Therefore, for $j = 1,2$, two mutual controlled Duffing circuits in Fig. 1 can be expressed as

$$\begin{aligned}\frac{d}{dt}\varphi_j &= U_{NL,j},\\ \frac{d}{dt}U_{NL,j} &= -\varepsilon U_{NL,j} - \varphi_j - \upsilon\varphi_j^3\\ &\quad + \mathbb{E}\cos\omega_0 t + \varepsilon K(U_{NL,3-j} - U_{NL,j}). \quad (8)\end{aligned}$$

The Coulomb interaction provides an additional potential energy, $\omega_m\eta' V_L(b^\dagger + b)^2/4$, to the oscillator, which has been deduced in Ref. [39]. Through utilizing a similar dimensionless transformation, the additional potential energy corresponding to the jth oscillator can be gained:

$$H_{ej} = \frac{\omega_m j}{4}\eta U_{NL,j}(b_j^\dagger + b_j)^2 \equiv \frac{\omega_m}{4}C_j(t)(b_j^\dagger + b_j)^2, \quad (9)$$

with the definition $C_j = \eta U_{NL,j}$ and the characteristic parameter

$$\eta = \sqrt{\frac{\chi_1}{c}}\phi_0\eta' = \frac{C_0 Q_{MR}\phi_0}{\pi\varepsilon_0 m\omega_m^2 d^3}\sqrt{\frac{\chi_1}{C}}. \quad (10)$$

Then the total Hamiltonian of this system can be expressed as ($\hbar = 1$)

$$\begin{aligned}H = \sum_{j=1,2}\Bigg\{&-\Delta_j a_j^\dagger a_j + \omega_{mj}\left[1 + \frac{C_j(t)}{2}\right]b_j^\dagger b_j\\ &- iga_j^\dagger a_j(b_j^\dagger + b_j) + iE(a_j^\dagger - a_j)\\ &+ \frac{\omega_{mj}}{4}C_j(t)(b_j^\dagger b_j^\dagger + b_j b_j)\Bigg\}\\ &- \mu(b_1^\dagger b_2 + b_2^\dagger b_1), \quad (11)\end{aligned}$$

after a frame rotating. Here for $j = 1,2$, a_j ($a_j^\dagger$) and b_j ($b_j^\dagger$) are the optical and mechanical annihilation (creation) operators. $\Delta_j = \omega_{dj} - \omega_{lj}$ refers to the detuning between the frequencies belonging, respectively, to the laser driving and the cavity mode. ω_{mj} is the mechanical frequency. g is the optomechanical coupling constant, and E is the driving intensity.

Generally speaking, the properties and trajectory of a quantum system corresponding to Hamiltonian (11) can be expressed completely by a density matrix through solving the quantum master equation in the Schrödinger picture. However, a CV quantum system usually corresponds to a density matrix with infinite dimension in Fock space. Therefore in order to avoid calculating a density matrix, in this work, we consider the dissipative effects in the Heisenberg picture and write the quantum Langevin equations to investigate the quantum trajectory of our system. Compared to the master equation, quantum Langevin equations can describe systematic dynamics through analyzing the evolutions of the system operators instead of solving a density matrix, and the quantum noise can be introduced into the motion equations based on input-output theory. Some common quantum properties, such as quantum fidelity and quantum entanglement, have been well calculated and discussed in previous works by adopting quantum Langevin equations [45–48]. Corresponding to the Hamiltonian in Eq. (11), the quantum Langevin equations of the operator motions are [36,49]

$$\begin{aligned}\dot{a}_j &= [-\kappa + i\Delta_j + ig(b_j^\dagger + b_j)]a_j + E + \sqrt{2\kappa}a_j^{in},\\ \dot{b}_j &= \left\{-\gamma - i\omega_{mj}\left[1 + \frac{C_j(t)}{2}\right]\right\}b_j + iga_j^\dagger a_j + i\mu b_{3-j}\\ &\quad - i\frac{\omega_{mj}}{2}C_j(t)b_j^\dagger + \sqrt{2\gamma}b_j^{in}. \quad (12)\end{aligned}$$

In this expression, κ and γ are the optical and mechanical damping rates, respectively, and a_j^{in} and b_j^{in} are the input bath operators. Under the Markovian approximation, the input operators are assumed to be white Gaussian fields obeying standard correlation: $\langle a_j^{in,\dagger}(t)a_{j'}^{in}(t') + a_{j'}^{in}(t')a_j^{in,\dagger}(t)\rangle = \delta_{jj'}\delta(t-t')$ [50] and $\langle b_j^{in,\dagger}(t)b_{j'}^{in}(t') + b_{j'}^{in}(t')b_j^{in,\dagger}(t)\rangle = (2\bar{n}_b + 1)\delta_{jj'}\delta(t-t')$, where $\bar{n}_b = [\exp(\hbar\omega_m j/k_B T) - 1]^{-1}$ is the mean phonon number of the mechanical bath, which gauges the temperature T [51].

Here we adopt mean-field approximation to simplify the above nonlinear differential operator equations since it is quite difficult to directly solve them [6,14,52–54]. Therefore, each operator in a quantum Langevin equation is expanded as the sum of a c number mean value and a fluctuation operator: $a_j(t) = \langle a_j(t)\rangle + [a_j(t) - \langle a_j(t)\rangle] := A_j(t) + \delta a_j$ and $b_j(t) := B_j(t) + \delta b_j$. Under a strong laser driving, the fluctuation can be regarded as a perturbation around the corresponding mean value. In this case, Eq. (12) can be divided into two different sets of equations, that is, for the mean value:

$$\begin{aligned}\dot{A}_j &= [-\kappa + i\Delta_j + ig(B_j^* + B_j)]A_j + E,\\ \dot{B}_j &= \left\{-\gamma - i\omega_{mj}\left[1 + \frac{C_j(t)}{2}\right]\right\}B_j + ig|A_j|^2 + i\mu B_{3-j}\\ &\quad - i\frac{\omega_m}{2}C_j(t)B_j^*, \quad (13)\end{aligned}$$

and for the fluctuation:

$$\begin{aligned}\delta\dot{a}_j &= [-\kappa + i\Delta_j + ig(B_j^* + B_j)]\delta a_j \\ &\quad + igA_j(\delta b_j^\dagger + \delta b_j) + \sqrt{2\kappa}a_j^{in}, \\ \delta\dot{b}_j &= \left\{-\gamma - i\omega_{mj}\left[1 + \frac{C_j(t)}{2}\right]\right\}\delta b_j + igA_j\delta a_j^\dagger \\ &\quad + igA_j^*\delta a_j + i\mu\delta b_{3-j} - i\frac{\omega_m}{2}C_j(t)\delta b_j^\dagger + \sqrt{2\gamma}b_j^{in}.\end{aligned} \tag{14}$$

In the above expressions, the quantum fluctuations have been already linearized by neglecting all second-order terms. Utilizing a mean-field approximation, except for convenience, is also based on the following two considerations. One is that quantum synchronization measure is of a clearer physical significance. Here we wish to emphasize once again that the synchronization in the level of expectation value in this case can be regarded as a necessary condition of quantum synchronization. The other is that mean-field approximation neglects the nonlinear effect in the quantum level, which causes the quantum properties of the system to be restricted to linear transformation. In our work, this characteristic can ensure that the system is always a Gaussian state [55]. It is the reason why the Gaussian fidelity and the Gaussian entanglement are accurate in the following discussion.

After transforming the annihilation and creation operators by using $\hat{x}_j = (a_j^\dagger + a_j)/\sqrt{2}$, $\hat{y}_j = i(a_j^\dagger - a_j)/\sqrt{2}$, $\hat{q}_j = (b_j^\dagger + b_j)/\sqrt{2}$, and $\hat{p}_j = i(b_j^\dagger - b_j)/\sqrt{2}$, Eq. (14) can be rewritten in a more compact form: $\partial_t\hat{u} = S\hat{u} + \hat{\xi}$. Here vector $\hat{u}$ is defined as $\hat{u} = (\delta x_1, \delta y_1, \delta x_2, \delta y_2, \delta q_1, \delta p_1, \delta q_2, \delta p_2)^\top$ and $\hat{\xi}$ means input vector $(\hat{x}_1^{in}, \hat{y}_1^{in}, \hat{x}_2^{in}, \hat{y}_2^{in}, \hat{q}_1^{in}, \hat{p}_1^{in}, \hat{q}_2^{in}, \hat{p}_2^{in})^\top$. S is a time-dependent coefficient matrix, and it can be solved by dynamic equations of the mean values (see Appendix B). In order to analyze quantum synchronization and quantum correlation, we consider the following covariance matrix:

$$V_{ij}(t) = V_{ji}(t) = \tfrac{1}{2}\langle\hat{u}_i(t)\hat{u}_j(t) + \hat{u}_j(t)\hat{u}_i(t)\rangle, \tag{15}$$

and its evolution satisfies [36]

$$\partial_t V = SV + VS^\top + N. \tag{16}$$

In the above expression, N is a diagonal noise correlation matrix $N_{ij}\delta(t-t') = \langle\hat{\xi}_i(t)\hat{\xi}_j(t') + \hat{\xi}_j(t')\hat{\xi}_i(t)\rangle/2$. Here we want to explain again that the expectation value of a mechanical quantity and the covariance matrix V can completely describe the system quantum properties if the system is restricted to the Gaussian state by the linearized Hamiltonian. According to Eqs. (8), (10), (13), and (16), the first-order synchronization measure between two oscillators can be obtained by $\langle q_-\rangle = \mathrm{Re}[B_1] - \mathrm{Re}[B_2]$ and $\langle p_-\rangle = \mathrm{Im}[B_1] - \mathrm{Im}[B_2]$. In addition, the second-order synchronization measure is

$$\begin{aligned}S_c'(t) &= \langle\delta\hat{q}_-^2(t) + \delta\hat{p}_-^2(t)\rangle^{-1} \\ &= \left\{\tfrac{1}{2}[V_{55}(t) + V_{77}(t) - 2V_{57}(t)]\right. \\ &\quad \left. + \tfrac{1}{2}[V_{66}(t) + V_{88}(t) - 2V_{68}(t)]\right\}^{-1}.\end{aligned} \tag{17}$$

With the covariance matrix in Eq. (15), the fidelity of two general Gaussian states can be obtained using the following formula [56,57]:

$$\mathcal{F} = \frac{2}{\sqrt{\Lambda + \lambda} - \sqrt{\lambda}}\exp[-\beta^\top(V_1 + V_2)^{-1}\beta], \tag{18}$$

where

$$V_1 = \begin{pmatrix} V_{11} & V_{12} \\ V_{21} & V_{22}\end{pmatrix}, \quad V_2 = \begin{pmatrix} V_{33} & V_{34} \\ V_{43} & V_{44}\end{pmatrix}, \tag{19}$$

$$\beta = \sqrt{2}\begin{pmatrix}\mathrm{Re}A_1 - \mathrm{Re}A_2 \\ \mathrm{Im}A_1 - \mathrm{Im}A_2\end{pmatrix}, \tag{20}$$

$$\Lambda = \det(V_1 + V_2), \tag{21}$$

and

$$\lambda = (\det V_1 - 1)(\det V_2 - 1). \tag{22}$$

Besides the quantum fidelity, we can also adopt the covariance matrix to calculate *logarithmic negativity*, which is a well-known measure to describe the entanglement between two Gaussian states. For convenience, we express the covariance matrix V in the following compact form:

$$V = \begin{pmatrix} I_{O1} & D_{O1,O2} & D_{O1,M1} & D_{O1,M2} \\ D_{O2,O1} & I_{O2} & D_{O2,M1} & D_{O2,M2} \\ D_{M1,O1} & D_{M1,O2} & I_{M1} & D_{M1,M2} \\ D_{M2,O1} & D_{M2,O2} & D_{M2,M1} & I_{M2}\end{pmatrix}, \tag{23}$$

where I_i and D_{ij} are 2×2 matrices. Here we use the indices O and M to specify the mechanical and optical modes; moreover, (i,j) denotes the entanglement between the modes i and j. For example, "(O_1, M_1)" means the entanglement between the optical mode and the mechanical mode of the system 1, correspondingly, and "(M_1, M_2)" is the entanglement between the mechanical modes of the systems 1 and 2. The covariance matrix of two entangled modes in this case can be written as

$$\nu_{ij} = \begin{pmatrix} I_i & D_{i,j} \\ D_{j,i} & I_j\end{pmatrix}, \tag{24}$$

and the *logarithmic negativity* can be calculated based on

$$E_N^{i,j} = \max[0, -\ln(2\zeta_{ij})]. \tag{25}$$

In this expression, ζ_{ij} is the smallest symplectic eigenvalue of the partially transposed covariance matrix $\tilde{\nu}_{ij}$ that can be obtained from ν_{ij} just by taking p_j in $-p_j$ [58,59]. This symplectic eigenvalue can be gained by calculating the square roots of the ordinary eigenvalues of $-(\sigma\tilde{\nu}_{ij})^2$, where $\sigma = J \oplus J$ and J is a 2×2 matrix with $J_{12} = -J_{21} = 1$ and $J_{11} = J_{22} = 0$.

IV. POINT-TO-POINT QUANTUM SYNCHRONIZATION AND STATE SHARING

We first consider point-to-point quantum state sharing between two systems connected directly (see Fig. 1). Two cavities here are the carriers of quantum states, and we hope to prepare identical unknown states via quantum synchronization oscillators. Because of the linearization for the quantum fluctuation, the systems can be described by Eqs. (8), (13), and (14) completely. By computing the covariance matrix of

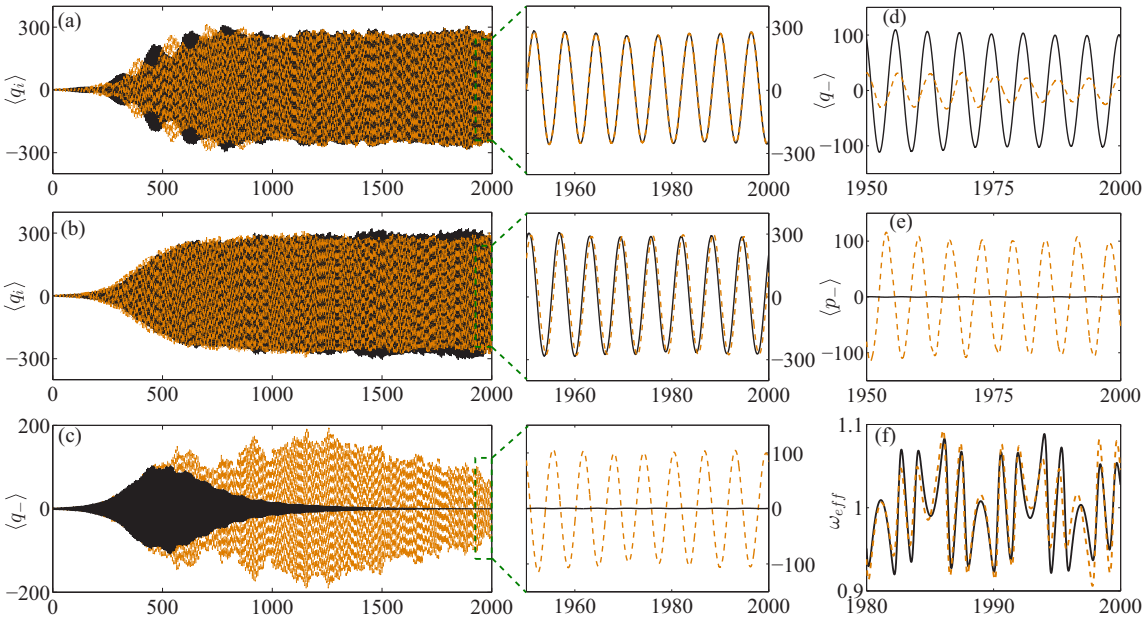

FIG. 2. (a), (b) Expectation values of the oscillator coordinates corresponding to existing (a) or disconnecting (b) of coupling. Here black solid lines denote $\langle q_1 \rangle$, and yellow dotted lines denote $\langle q_2 \rangle$. (c), (d) Expectation values of the coordinate error operator corresponding to $K = 2$, $\mu = 0.02$ (c, black solid); $K = 0$, $\mu = 0$ (c, yellow dotted); $K = 2$, $\mu = 0$ (d, black solid); and $K = 0$, $\mu = 0.02$ (d, yellow dotted). (e) Expectation values of the momentum error operator corresponding to $K = 2$, $\mu = 0.02$ (black solid) and $K = 0$, $\mu = 0$ (yellow dotted). (f) Effective frequencies of system 1 (yellow dotted) and 2 (black solid) when $K = 0$. In these simulations, the oscillator frequency is set $\omega_{m1} = 1$ as a unit, and other parameters are $\omega_{m2} = 1$, $\omega_0 = 0.8$, $\Delta_j = \omega_{mj} = 1$, $g = 0.005$, $\kappa = 0.15$, $\gamma = 0.005$, $\eta = 0.01$, $\varepsilon = 0.18$, $\nu = 1$, $E = 10$, and $\mathbb{E} = 26.7$. The initial state of the cavity field is vacuum state which corresponds to $A_j(0) = 0$, and other initial conditions are all random. All horizontal coordinates denote time t.

the systems, the evolution of the synchronization measure in Eq. (3) can be calculated conveniently. Since the oscillators are directly coupled, we use nonlocal measure S_c' to describe oscillator synchronization. For cavity fields, quantum sharing is more concerned with the consistency of the local quantum states in each cavity. Hence, we use local measure fidelity to describe optical fields.

In Fig. 2 we show the dynamics of oscillators by plotting the evolutions of the operator expectation values. One can obviously see that synchronous evolution between the oscillators appears under the suitable coupling intensity [Fig. 2(a)], but this synchronization will be destroyed when both couplings are disconnected [Fig. 2(b)] and two evolution curves are inconsistent. In Figs. 2(c) and 2(d), we demonstrate this phenomenon more intuitively by considering the first-order error $\langle q_- \rangle = \langle q_1 \rangle - \langle q_2 \rangle$. Here $\langle q_- \rangle$ is plotted under different connections, and it shows that the error will always tend to zero if and only if two couplings exist simultaneously [black solid line in (c)]. Otherwise, the error will take on irregular evolution with large amplitude [(d) and dotted line in (c)]. Figure 2(e) illustrates that all the conclusions obtained from the generalized coordinate can also be applied to the generalized momentum. In Fig. 2(f), we plot the effective frequency ω_{eff} of each subsystem to illustrate the significant difference between two systems when $K = 0$.

While $\langle q_- \rangle \to 0$ and $\langle p_- \rangle \to 0$ are simultaneously satisfied, two oscillators will exhibit the characteristics of complete synchronization in the level of expectation value. In some previous works, this kind of synchronization is also considered as a quantum synchronization. This view is not strict because the expectation value is an incomplete description without considering quantum fluctuation. If the synchronization is not intended to be used in semiclassical information processing (e.g., transmission of strong signal and parameter identification in quantum ensemble) but needs more quantum properties, the nonlocality and quantum fluctuation will also cause a critical impact, and they cannot be ignored in quantum synchronization analyses. In particular, for the Gaussian state sharing discussed in our work, a genuine quantum synchronization will be required.

In Fig. 3 we present the contrast among the expectation value synchronization, quantum synchronization, and Gaussian fidelity [56,57]. Compared with only considering the expectation value, here evolution of the system is more complicated and can be subdivided into three distinguishable processes according to the quantum synchronization measure S_c'. First, two systems are not synchronized because there obviously exists a classical error between oscillator expectation values. Correspondingly, S_c' always tends to 0. Subsequently, with the classic error gradually tending to zero, S_c' also gradually increases with time evolution at this stage. The gradually rising S_c' illustrates that this process is a transformation process from quantum nonsynchronization to quantum synchronization. Physically, the appearance of this process is due to the mutual modulation between two systems. From Fig. 3(c), we find that the corresponding fidelity of two cavity fields is also rising in this duration, but it is not yet available for quantum sharing. With the evolution continuing

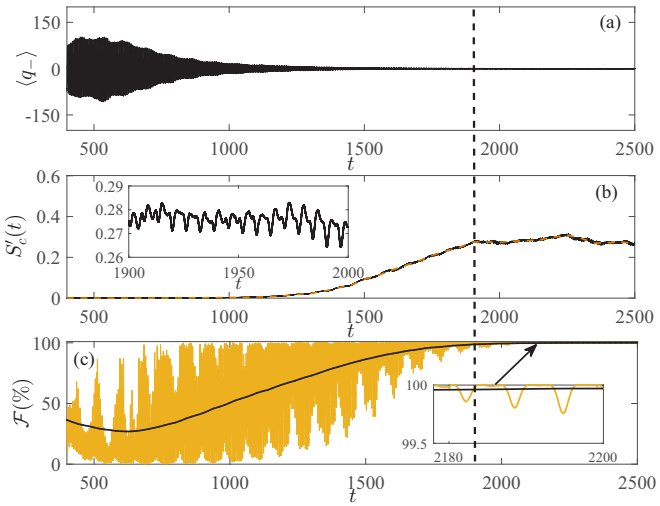

FIG. 3. Simulations of the expectation value error $\langle q_- \rangle$, quantum synchronization measure $S_c'(t)$, and Gaussian fidelity $\mathcal{F}$. The inset in (b) is the partial enlarged drawing of S_c' in $t \in [1900, 2000]$. In (b) and (c), the yellow (pale) lines express the local average synchronization measure and Gaussian fidelity by calculating $\bar{\xi}(\bar{t}) = \Delta t^{-1} \int_t^{t+\Delta t} \xi \, dt$ in the time window Δt ($\xi \in \{S_c', \mathcal{F}\}$); Here all the other parameters are the same as in Fig. 2.

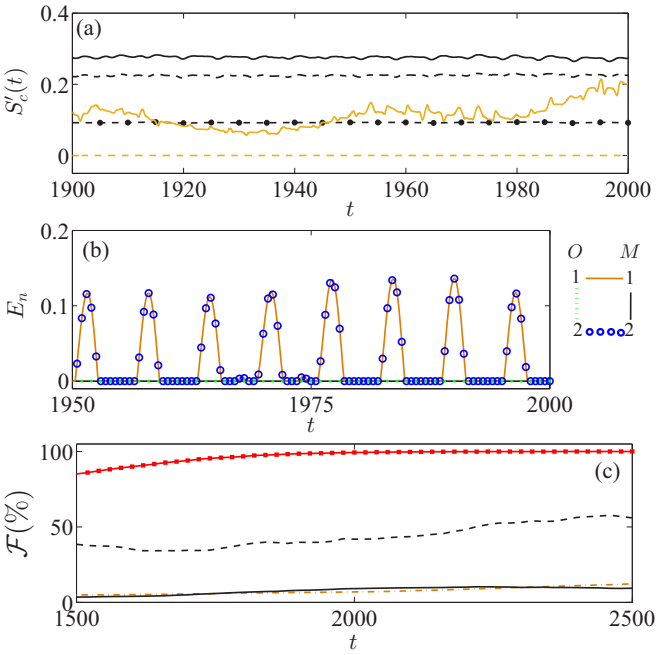

FIG. 4. (a) Quantum synchronization measures under different conditions. Here black (dark) lines denote S_c' when $\bar{n}_b = 0$ (solid), $\bar{n}_b = 0.25$ (dotted), and $\bar{n}_b = 2.5$ (circle). Yellow (pale) lines denote S_c' under $K = 0$, $\mu = 0.02$ (solid), and $K = 0$, $\mu = 0$ (dotted). (b) Evolution of *logarithmic negativity*. (c) Local averaged fidelities, respectively, corresponding to $K = 2$, $\mu = 0.02$ (red square); $K = 2$, $\mu = 0$ (yellow (pale) dotted); $K = 0$, $\mu = 0.02$ (black (dark) dashed); and $K = 0$, $\mu = 0$ (black (dark) solid). Here all the other parameters are the same as in Fig. 2.

and finally for S_c', an inflection point appears (see the dotted boundary line). After this inflection point, a stable nonzero S_c' emerges and in maintained in a long time interval, and the corresponding fidelity tends to 100%, which implies two cavity fields evolve gradually from vacuum states to the quantum states with almost 100% reliability. The inset in Fig. 3(b) shows that S_c' is greater than 0.26 after the inflection point, which is a higher value compared to Mari's results. It can be certain from above analyses that quantum fluctuation can be regarded as synchronization in this process.

In Fig. 4(a) we show quantum synchronization measures under different conditions. The results show that S_c' will decrease to 0.1 when the classical coupling is disconnected. Although S_c' is unequal to zero in this case, it does not mean that the systems have been synchronized because the classical error will no longer tend to zero [see Fig. 2(d)]. Moreover, S_c' will equal zero if both couplings are disconnected. By comparing these two results, it can be proved that the quantum coupling is more suitable for playing a role in restraining the difference between the quantum fluctuations. Similar conclusions can also be verified by Fig. 4(c), which shows that $\mathcal{F}(\infty) \to 100\%$ will be satisfied only while both two couplings are connected synchronously. Figure 4(a) also shows that this synchronization will keep high efficiency if the bath temperature is limited to be lower than $T = 1\,\mathrm{mK}$ (corresponding to MHz phonon frequency). Moreover, S_c' will still be greater than 0.1 even when $T = 5\,\mathrm{mK}$, which corresponds to a strong robustness. Another concern in this work is whether the quantum properties of two systems are also identical at the synchronization moment. Therefore, we plot Fig. 4(b) and confirm that the entanglement of two systems also takes on consistent evolution. Considering the above properties together, we can finally determine that the synchronization between two systems indeed belongs to a genuine quantum synchronization. Figure 4(b) also illustrates the two systems are always separable in both optical field and oscillator freedoms. This characteristic is suitable for a quantum network because other nodes will be not disturbed by entanglement steering when a node is attacked or bugged.

Figures 2(c), 2(d), and 4(c) illustrate that the couplings via a phonon channel and linear resistor in our model are both necessary for synchronization. This feature has rarely been used to design synchronization schemes in previous works. In fact, these two kinds of couplings respectively exhibit different physical mechanisms in the synchronization process. Here quantum coupling plays a similar role as that reported in Ref. [14], i.e., it is used to eliminate the initial difference between two identical systems by mutual adjustment and to generate nonlocality in order to improve the synchronization measure. However, different from Ref. [14], every subsystem in our work can be treated as the same if and only if circuit coupling is connected. In other words, the synchronization mechanisms in our paper are as follows: Circuit coupling controls subsystems eventually have the same effective frequency, which means two subsystems evolve under the same dynamic equation. Once this condition is satisfied, the responsibility of phonon coupling is to offset the initial difference between two subsystems. On the other hand, if circuit coupling is disconnected or one of the subsystems is a common optomechanical system without control voltage ($\omega_{\mathrm{eff}} = \omega_m$),

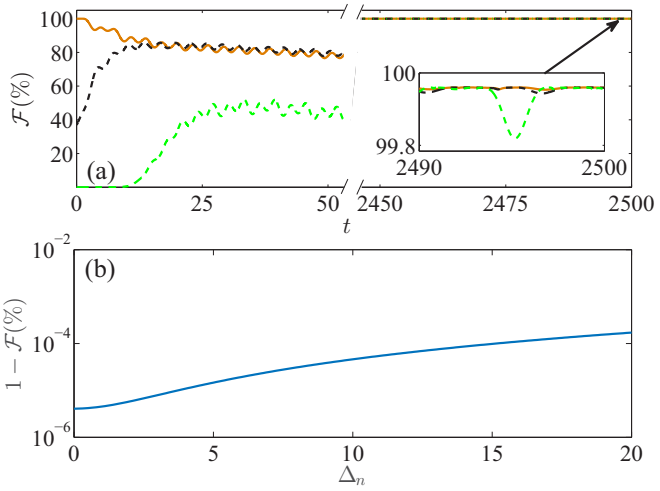

FIG. 5. (a) Initial state dependency of fidelity. The initial states of cavity fields are respectively selected as two vacuum states: $|0\rangle$ and $|0\rangle$ (yellow solid); coherent states with identical photon number: $|\alpha\rangle$ and $|\alpha e^{i\phi}\rangle$ (black dark dashed); and coherent states with different photon number: $|\alpha_1\rangle$ and $|\alpha_2\rangle$ (green light dotted). Here $|\alpha\rangle = \exp(\alpha a^\dagger - \alpha^* a)|0\rangle$, $\alpha = \alpha_1 = 1$, $\alpha_2 = 10$, and $\phi = \pi/2$. (b) Gaussian fidelities with varied phonon number difference. Here we set $\bar{n}_{b1} + \bar{n}_{b2} = 20$, $\Delta n = \bar{n}_{b1} - \bar{n}_{b2}$, and all the other parameters are the same as in Fig. 2.

dynamic equations of the two systems are different and exhibit unequal effective frequencies [see Fig. 2(f)]. In this case, weak quantum coupling will not be sufficient to synchronize two different systems. Compared to related works that obtain quantum synchronizations by only one coupling, our scheme can ensure a wide range of achievable parameters since the quantum coupling is responsible only for synchronizing the initial difference. At the same time, two kinds of couplings can provide an additional control mode. Both the wider range of parameters and the additional control mode can make the constructing of network more convenient.

To show the efficiency of the state sharing, finally, we end the analysis of a point-to-point system by discussing the initial state dependence and environment influence on Gaussian fidelity. In Fig. 5(a) we plot the evolutions of the fidelity with different initial states. It can be known that $\mathcal{F}(\infty) \to 100\%$ can always be achieved even starting evolution from an arbitrary initial state. This is because the synchronization effect is an intrinsic property of the system, and it is irrelevant with the initial selection. Figure 5(b) illustrates that the cavity field fidelity will always tend to 100% even though the corresponding oscillators are dissipating into different baths. This property is quite different with S_c', which takes on an obvious decline once the phonon number within bath increases. This is due to the fact that the influence of bath on the system has be simplified as a decay parameter under the Markovian approximation, and such a kind of parametric difference is also balanced by the quantum coupling when the optomechanical interaction and system-bath interaction are both weak. This performance will relax the requirement for the experimental conditions; in other words, it is more feasible to extend the idea of quantum state sharing from the point-to-point system to the quantum network.

V. QUANTUM SYNCHRONIZATION AND STATE SHARING IN A COMPLEX NETWORK

Now let us extend the above conclusions to analyze state sharing within the network. Similarly to the discussion about a point-to-point system, we also begin this section with a dynamic analysis of a hybrid electro-optomechanical system array. According to Eq. (11), the whole Hamiltonian of a quantum network can be expressed as

$$\begin{aligned} H &= H_{\text{free}} + H_{\text{couple}} \\ &= \sum_{i=1}^{N} \left\{ -\Delta_i a_i^\dagger a_i + \omega_{mi}\left[1+\frac{C_i(t)}{2}\right] b_i^\dagger b_i - i g a_i^\dagger a_i (b_i^\dagger + b_i) \right. \\ &\quad \left. + iE(a_i^\dagger - a_i) + \frac{\omega_{mi}}{4} C_j(t)(b_i^\dagger b_i^\dagger + b_i b_i) \right\} \\ &\quad - \sum_{t,q} \mu_{jk}(b_j^\dagger b_k + b_k^\dagger b_j), \end{aligned} \tag{26}$$

where N is the total number of nodes and μ_{jk} represents the coupling strength between nodes j and k. Here $C_i(t)$ can be determined by Duffing circuit equations

$$\begin{aligned} \dot{\varphi}_i &= U_{NL,i}, \\ \dot{U}_{NL,i} &= -\varepsilon U_{NL,i} - \varphi_i - \upsilon \varphi_i^3 + \mathbb{E}\cos\omega_0 t \\ &\quad + \sum_{t,c}^{k=i} \varepsilon K_{jk}(U_{NL,j} - U_{NL,i}), \end{aligned} \tag{27}$$

and, correspondingly, other mechanical quantities satisfy the following quantum Langevin equations:

$$\begin{aligned} \dot{a}_j &= [-\kappa + i\Delta_j + ig(b_j^\dagger + b_j)]a_j + E + \sqrt{2\kappa}a_j^{in} \\ \dot{b}_j &= \left\{ -\gamma - i\omega_{mj}\left[1+\frac{C_j(t)}{2}\right] \right\} b_j + i g a_j^\dagger a_j - i\frac{\omega_{mj}}{2} C_j(t) b_j^\dagger \\ &\quad + \sum_{t,q}^{j=i} i\mu_{jk} b_k + \sqrt{2\gamma} b_j^{in}. \end{aligned} \tag{28}$$

After a mean-field approximation, Eq. (28) becomes

$$\begin{aligned} \dot{A}_i &= [-\kappa + i\Delta_i + ig(B_i^* + B_i)]A_i + E, \\ \dot{B}_i &= \left\{ -\gamma - i\omega_{mi}\left[1+\frac{C_i(t)}{2}\right] \right\} B_i + ig|A_i|^2 \\ &\quad - i\frac{\omega_m}{2} C_i(t) B_i^* + \sum_{t,q}^{j=i} i\mu_{jk} B_k, \end{aligned} \tag{29}$$

to describe the evolution of expected value. Here we define two graph matrices, $G_{jk}^c = K_{jk}$ and $G_{jk}^q = \mu_{jk}$, to represent the coupling structures of circuit coupling and phonon coupling, respectively. G^c can be an arbitrary matrix since circuit coupling is classical; however, the Hermitian Hamiltonian requires $(G^q)^\top = G^q$. Based on this expression, Eqs. (27) and (28) can be rewritten in a more compact form by using graph matrices [60]:

$$\dot{\mathbf{X}} = F(\mathbf{X}) + G^c(t) \otimes H_c \cdot \mathbf{X} + iG^q(t) \otimes H_q \cdot \mathbf{X}. \tag{30}$$

In this expression, $\mathbf{X} = (\mathbf{X}^1, \mathbf{X}^2, \mathbf{X}^3, \ldots, \mathbf{X}^N)^\top$ is defined as a network tensor, where $\mathbf{X}^j = (\phi_j, U_{NL,j}, A_j, B_j)$. The second

term and the third term on the right side respectively correspond to classical coupling term $\sum_{t,c} \varepsilon K(U_{NL,j} - U_{NL,i})$ and quantum coupling $\sum_{t,q}^{j=i} i\mu_{jk} B_k$, and $F(\mathbf{X})$ describing free evolution of each node includes the remaining parts of Eqs. (27) and (28). H_c and H_q refer to the autocorrelation functions that describe the nexus between the variables in the same node. If the variable order is defined as $\mathbf{X}^j = (\phi_j, U_{NL,j}, A_j, B_j)$, the autocorrelation functions should be $H_c = \mathrm{diag}(0,1,0,0)$ and $H_q = \mathrm{diag}(0,0,0,1)$.

With the advances of network theory, it is gradually known that the irregular but incompletely random network is better and more practical than other network structures for application in communication or calculation process. In the last few decades, the small-world (SW) network and the scale-free (SF) network have been widely investigated and can act as effective simulations of actual communication networks. This motivates us to propose synchronization schemes for an SW network and SF network in the following subsections, respectively. The SW network corresponds to the case that only few directly connected nodes in network are achieved for synchronization. In addition, it is not required to design additional controls for synchronization in an SW network. If the synchronization target is used to synchronize all nodes in an irregular network, we need a designed synchronization condition to adjust the parameters of each node, which is the goal of the synchronization in an SF network.

A. Quantum synchronization in a small-world network

We now go into detail about quantum synchronization in an SW network. A typical Newman-Watts SW network can be regarded as adding a few irregular links in the frame of a regular network with neighboring links. The construction of such a network can be divided into two steps:

(1) *Establishing a regular network:* Staring from a ringlike network with regular connectivity comprising N nodes, and each node within the network connects to its M (even number) nearest neighbors.

(2) *Randomization edge adding:* In addition to the above links, each node can also connect to non-nearest-neighbor nodes at random with small probability P.

For hybrid electro-optomechanical systems, the two above structures can, respectively, correspond to the classical coupling and quantum coupling. As shown in Fig. 6(a), we construct an SW network with the following strategy: N electro-optomechanical systems (orange big points) are selected as the nodes of the network, and their circuit parts link to the nearest-neighbor nodes via classical Duffing couplings (blue dotted lines). A node will not link any other nodes via quantum couplings (red solid lines) unless it wants to synchronize with other nodes. In our small-world network, time-dependent topology refers to that a node can select different nodes for quantum coupling in the time evolution [see Fig. 6(b)].

In the case of larger N, the quantum coupling here can be regarded as random connection with a small probability P. Previous works have proved that such a network topology is of smaller average path length and larger clustering coefficient [61,62]. To some extent, an SW network remains symmetry like a regular network, and the node differences caused by

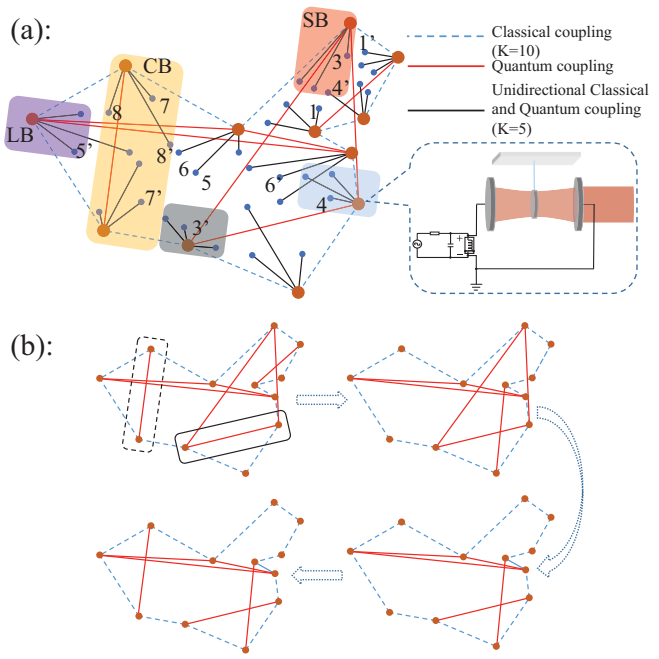

FIG. 6. Each node represents an eletro-optomechanical system. The nodes connect to each other through different coupling forms and dissipate into different baths, including a separate bath (SB), common bath (CB), and local bath (LB). Here (a) represents the structure of the SW network consisting of primary and secondary nodes and (b) shows a SW network with varying structure.

network topology are small enough to be eliminated because of the weak coupling in the quantum domain. Especially when N and P are fixed, the change of the network structure will have a tiny impact on direct connected nodes, which ensures that quantum synchronization can be extended more conveniently into an SW network.

Now we discuss the above analyses in mathematics. Let us reexamine the dynamic equation (30). In view of an SW network, elements of G^c should be zero except $g^c_{i,i\pm1} = \varepsilon K$ and $g^c_{1,N} = g^c_{N,1} = \varepsilon K$. Correspondingly, elements of G^q should perform as $g^q_{jk} = \mu_{jk}$. Substituting G^c and G^q into Eq. (30), the dynamics of the whole network can be determined by coupling matrix

$$G_{N,M,P}(t) = G^c(t) \otimes H_c + iG^q(t) \otimes H_q. \tag{31}$$

We can calculate the trace distance under a different time,

$$D(t,t') = \frac{1}{2}\mathrm{Tr}\left| \frac{G_{N,M,P}(t)}{|G_{N,M,P}(t)|} - \frac{G_{N,M,P}(t')}{|G_{N,M,P}(t')|} \right|, \tag{32}$$

to measure the difference between two different coupling matrices. Under fixed network parameters, the influence caused by the changing network structure on synchronization can be measured by using average distance $\bar{D}(N,M,P) = [\int_{t_0}^{t} D(t_0,\tau)\,d\tau]/(t-t_0)$. Here $|A|$ is defined as $\sqrt{A^\dagger A}$.

As illustrated in Fig. 7(a), the average distance of an SW network with $N = 12$ and $P = 0.1$ will decrease with increasing the quantum coupling intensity μ. Especially corresponding to $\mu = 0.02$, $\bar{D}$ is approximately equal to 0.01, and it will be less than 0.015 even when $P = 0.3$ [see inset in Fig. 7(a)]. Such a small difference indicates that quantum coupled nodes can

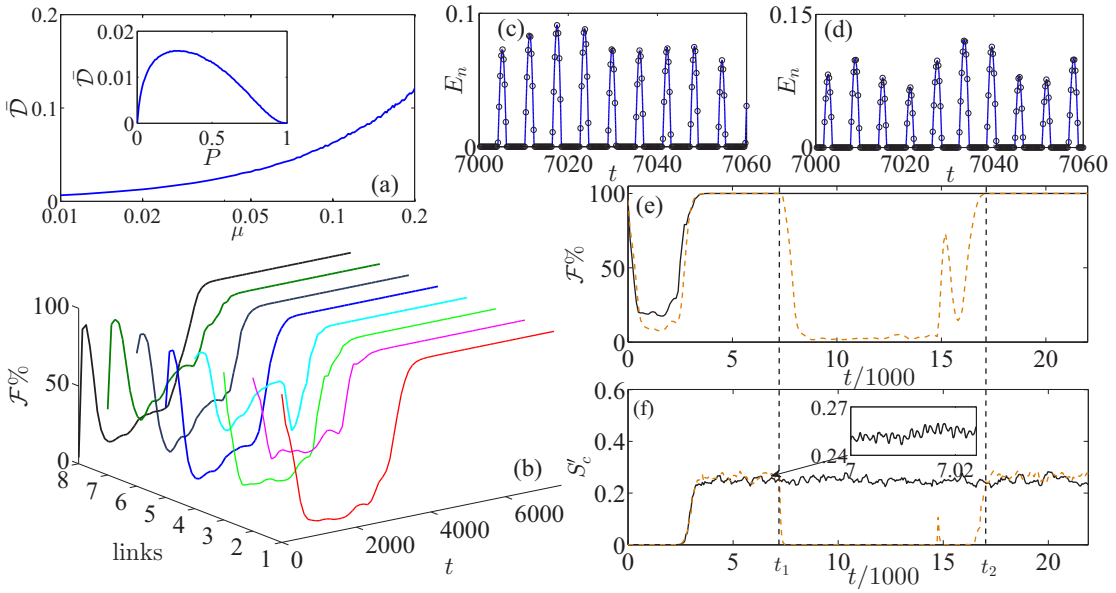

FIG. 7. (a) Average trace distance $\bar{D}$ with varied coupling intensity μ under $N = 12$, $M = 2$, and $P = 0.1$. The inset in (a) shows change of $\bar{D}$ with varied edge-adding probability P under $N = 12$, $M = 2$, and $\mu = 0.02$. (b) Fidelities between two nodes in different linear motifs. Here link i refers to the connection between nodes i and i' in Fig. 6(a). (c) and (d) Entanglement measures of the quantum states in different cavities. (e) and (f) Fidelities and synchronization measures between two nodes when the network structure varies. The yellow (dotted) line represents the link disconnects at t_1 and reconnects at t_2. The initial state of each cavity field is a vacuum state or random coherent mix state. Other initial conditions are all random, and all the other parameters are the same as in Fig. 2.

be directly synchronized without any additional control in an SW network.

In order to verify the above discussion, we calculate the dynamical evolution of a 12-node SW network [Fig. 6(a)]. We find that the network synchronization can be more efficient since each node can continue to synchronize other nodes. As an example, here each major node is known as a central node to derive the star-type network with S secondary nodes [blue small points in Fig. 6(a)]. In this case, we can still realize synchronously the synchronization among a large number of nodes even in an SW network.

In Fig. 7 we show the evolutions of optical field fidelity and field-oscillator entanglement of some key nodes dissipating into different baths. For each linear motif quantum coupling, the fidelity can stabilize at 100% for a long evolution time. Unlike an SF network and Erdös-Rényi random network [29,63], we emphasize that all nodes are directly connected to the network without modifying deliberately any parameters. Therefore the state sharing in this structure is quite convenient. Moreover, as we discussed in point-to-point processing, the differences caused by the bath influence can be eliminated by the coupling. It is further verified by the Fig. 7(b) that $\mathcal{F}(\infty) \to 100\%$ is always satisfied whether in SB, CB, or LB. Figures 7(c) and 7(d) illustrate that consistent quantum states belonging to different nodes are not thermal equilibrium states but have significant, not meaningless, quantum properties. The optical field and oscillator in each node are still entangled even if $t \to 7500$, and simultaneously, the *logarithmic negativity* is consistent between nodes in the same linear motif.

Now we discuss the synchronization performance when the network structure is constantly changing. Our aim is to prove that a state-sharing processing will not be affected by other processes in the same network. We consider such a process: two nodes are continuously connected [solid box in Fig. 6(b)], and in the meantime, other links [dotted box in Fig. 6(b)] are disconnected at t_1 and reconnected at t_2 [see dotted boundary lines in Figs. 7(e) and 7(f)]. It can be seen in Fig. 7(e) that the nodes with a continuous connection will continue to maintain synchronization and $\mathcal{F}(\infty) \to 100\%$ whether other links are connected or disconnected. It can be predicted that identical quantum states can be transmitted in this SW network even though its topology is varying with time. Similarly, we emphasize again that any parameter correction or additional control on nodes is not needed in this varying network. Therefore, any links can be established or broken off at any time. Moreover, we show that the disconnected nodes can also be synchronized when they are connected again in Fig. 7(f). The consistent evolution trends corresponding to fidelity and synchronization measure explain that quantum state sharing is present when synchronization arises.

B. Quantum synchronization in a scale-free network

The same protocol discussed above can be applied to synchronize few elements (two or three major nodes) of a network. However, it cannot ensure that many nodes can be synchronized simultaneously via complex connections. In particular, if a connected node constantly connects to other nodes or the probability of edge adding is not small, the whole network will become more complex and lose its symmetry. In this case, the whole network cannot be synchronized just through connecting directly nodes with each other. The potential scheme to synchronize asymmetric network requires us to modify the parameters of each local node.

To illustrate the problem, we consider a typical SF network as shown in Fig. 8(b). It starts from the network with m_0 nodes,

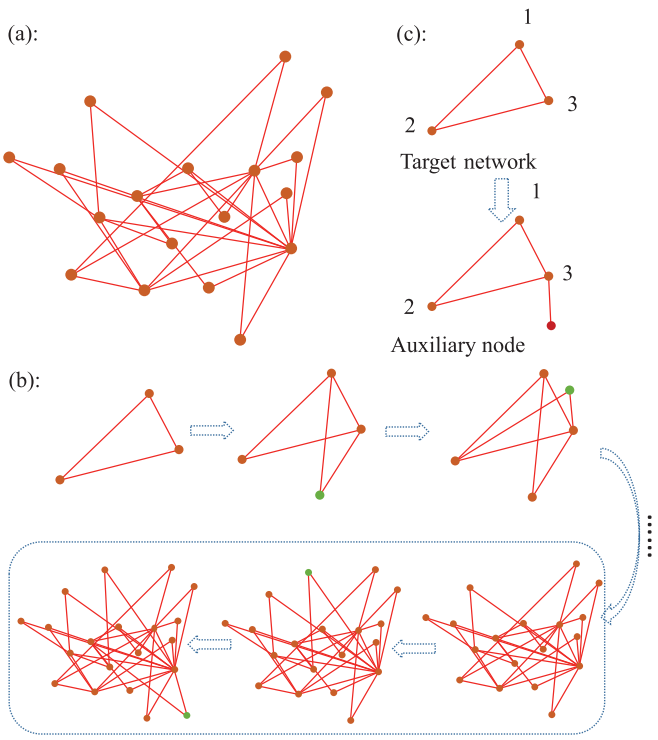

FIG. 8. (a) Structure diagram of an SF network with 18 nodes. (b) An SF network with a variable structure. (c) A simple example of network synchronization with an auxiliary node. Here the red solid lines represent the quantum couplings.

and in each subsequent process, a new node is added and connected to the network with m existing nodes ($m < m_0$). What needs to be explained is that the new node is apt to connect with such nodes with large node degree. Differently from the SW network, here time-dependent topology refers to new nodes accessing the network constantly.

In order to synchronize all nodes in such an SF network, here we introduce and adopt the dissipative condition, which can be expressed as

$$\sum_{k=1}^{N} g_{jk}^{q} = 0 \tag{33}$$

to control network synchronization [60,64]. Here g_{jk}^{q} is the element of coupling matrix G^q that describes a special coupling structure. Once the dissipative condition is satisfied, all quantum coupling terms in dynamic equation will no longer exist when all nodes have been synchronized. In order to explain this condition more clearly, let us rewrite Eq. (33) as $g_{jj} = -\sum_{k=1,k\neq j}^{N} g_{jk}$ and discuss its two sides. Considering the quantum Langevin equations, nondiagonal elements of the coupling matrix G^q correspond to the beam splitter (BS) terms $-\mu_{jk}(b_j^{\dagger}b_k + b_k^{\dagger}b_j)$, and conversely, diagonal elements g_{jj} can be regard as frequency shift terms $-\Delta\omega_j b_j^{\dagger}b_j$ in the Hamiltonian. Mathematically, those shift terms can express diverse frequencies of different nodes via setting a uniform reference frequency ω_s, i.e., $\omega_{mj} = \omega_s + \Delta\omega_j$. Besides the dissipative condition, an identical node function requires identical η for each node. Combining with these two requirements, we gain the conditions for whole network synchronization as follows:

$$\Delta\omega_j = \sum_{k=1}^{N} \mu_{jk} \quad \text{and} \quad \frac{Q_{MR,j}}{\omega_s + \Delta\omega_j} = \text{const}, \tag{34}$$

where ω_s should equal $\omega_s < \min\{\omega_{mj}\}$ owing to $\mu_{jk} > 0$. In this case Eq. (29) will reduce to

$$\begin{aligned}
\dot{A}_i &= [-\kappa + i\Delta_i + ig(B_i^* + B_i)]A_i + E, \\
\dot{B}_i &= \left\{-\gamma - i\omega_s\left[1 + \frac{C_i(t)}{2}\right]\right\}B_i + ig|A_i|^2 \\
&\quad - i\frac{\omega_s}{2}C_i(t)B_i^*,
\end{aligned} \tag{35}$$

owing to $B_i = B_j$ ($j \in [1,N], j \neq i$). Equation (35) implies that synchronization states can be determined only by respective node functions that have the same forms due to synchronized voltage control. The network evolution under this mechanism can be interpreted as follows: Different initial states and node functions will lead to initial differences among all nodes, which can be regarded as phase differences when the node functions are controlled with identical parameters. In phase space, mutual quantum coupling makes the error between two nodes take on periodic evolution in a weak nonlinear regime, which ensures that the systemic evolutionary track is a limit cycle but not chaos. Therefore, there is always such a moment (the least common multiple of the error periods) that all node errors simultaneously tend to zero. Once this phenomenon emerges, zero coupling terms and identical node functions ensure the system variables sustain synchronous state.

Note that the first equation in Eq. (34) is a nonidempotent linear equation, and it can not always be solved since Hermitian BS terms require $\mu_{jk} = \mu_{kj}$. To ensure that at least one solution exists, a simple method is to add some auxiliary nodes and connections into the network that should be designed for satisfying the solution condition. In other words, one can always find suitable parameters to ensure state sharing within the whole complex network.

In order to explain the synchronization conditions more intuitively, we discuss a triangle structure as an example to show how to adjust the coupling strength to satisfy the synchronization conditions [see Fig. 8(c)]. Considering this kind of triangular coupling structure, the first synchronization condition in Eq. (34) can be rewritten as

$$\begin{aligned}
\omega_{m1} - \omega_s &= \mu_{12} + \mu_{13}, \\
\omega_{m2} - \omega_s &= \mu_{12} + \mu_{23}, \\
\omega_{m3} - \omega_s &= \mu_{23} + \mu_{13}.
\end{aligned} \tag{36}$$

In the above expressions, $\omega_{m1,2,3}$ are oscillator frequencies of target nodes, and they should be arbitrary but fixed. Relatively, ω_s is a designed standard frequency, and it is similar to $\mu_{12,13,23}$, which can be adjusted according to different coupling structures or network parameters. Under normal circumstances, physical solutions may not exist for the equation while $\omega_{m1,2,3}$ are taken arbitrarily. As mentioned above, we add an auxiliary node and connection into the network to ensure the synchronization conditions can be satisfied. Considering the new structure consisting of the

auxiliary node, Eq. (36) becomes

$$\begin{aligned}\omega_{m1}-\omega_s &= \mu_{12}+\mu_{13},\\ \omega_{m2}-\omega_s &= \mu_{12}+\mu_{23},\\ \omega_{m3}-\omega_s &= \mu_{23}+\mu_{13}+\mu_A,\\ \omega_{mA}-\omega_s &= \mu_A,\end{aligned} \tag{37}$$

where ω_{mA} is the oscillator frequency of the auxiliary node. Equation (38) will exist with infinitely many solutions by properly selecting ω_A and μ_A. In particular, if we set

$$\begin{aligned}\omega_s &= \omega_{m1}-\mu_{12}-\mu_{13},\\ \mu_{23} &= \mu_{13}+\omega_{m2}-\omega_{m1},\\ \mu_A &= \mu_{12}-\mu_{13}+\omega_{m3}-\omega_{m2},\\ \omega_{mA} &= -2\mu_{13}+\omega_{m1}-\omega_{m2}+\omega_{m3},\end{aligned} \tag{38}$$

the dissipative condition will be satisfied even for arbitrary μ_{12} and μ_{13}.

In order to validate that the above ideas can be extended into complex networks, here we calculate the dynamical evolution of an 18-node SF network [Fig. 8(c)]. Quantum sharing within the network is measured and analyzed by a network-averaged fidelity defined as

$$\mathcal{F}(N)=\frac{\sum_{j<k}\mathcal{F}_{jk}}{C_N^2}. \tag{39}$$

Here $\mathcal{F}_{jk}$ is the fidelity of nodes j and k, and C_N^2 is the combination number. Under this definition, that $\mathcal{F}(N)$ tends to 100% means that the fidelity between any two nodes tends to 100% .

In Fig. 9(a) we show the evolution of network-averaged fidelity. It can be seen that $\mathcal{F}(N) > 99\%$ is always tenable, and time-averaged fidelity can achieve $\mathcal{F} = 99.53\%$ under the same parameters. Furthermore, the best result of quantum state sharing between two nodes can achieve $\mathcal{F} = 99.99\%$, and correspondingly, the worst synchronization effect between two nodes in this network can also ensure successful state sharing with $\mathcal{F} > 98.5\%$.

Now we focus on varying network structure. We consider joining two new nodes into the network one after another [corresponding to blue dashed box in Fig. 8(b)]. When new nodes are added, the network parameters will be adjusted to satisfy synchronization conditions under the new structure. In the general case, only the nodes that are directly connected with the new joining node need to be adjusted since the SF network requires new nodes to be added on the basis of the original structure. In Fig. 9(b) we exhibit that new nodes are not synchronized with other nodes when they are in the free evolution, and the fidelities between the new node and other nodes in the network remain at a lower value. Once a node accesses into the network [i.e., $t/1000 = 5$ in Fig. 9(b)], it will synchronize with other nodes rapidly, and the corresponding fidelity will continue to rise until it reaches almost 100%. For other nodes in the network, average fidelity shows that the new node will not affect the original synchronization effect although average fidelity decreases when new nodes just access into the network. We can also get the same conclusion by studying the synchronization measure of oscillators. As shown in Fig. 9(c), S_c' between a new node and any other nodes

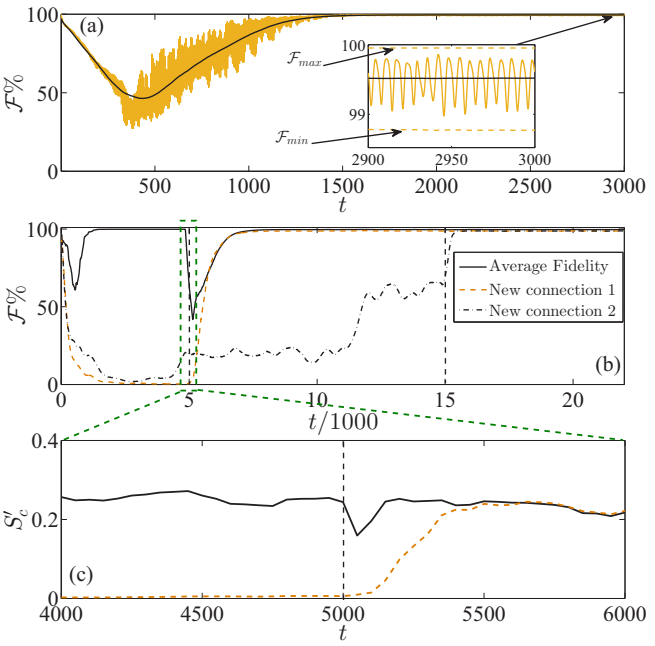

FIG. 9. (a) Network-averaged fidelity (black dark) and its local time average value (yellow pale). (b) Fidelities between two nodes when the network structure varies. (c) Quantum synchronization measures when the network structure varies and the time interval corresponds to the green box in (b). Here the initial state of each cavity field is vacuum state and other initial conditions are all random, and all the other parameters are the same as in Fig. 2.

has a significant improvement and finally stabilizes at 0.25, roughly. To summarize, we can ensure that the state-sharing processing can also work even if the network structure is varying. Finally, we plot the entanglement measures to further illustrate the nonclassical effect of the field in each node, shown in Fig. 10(a), and to show that $\mathcal{F}(\infty) \to 100\%$ can always be achieved, even when starting evolution from an arbitrary initial state, shown in Fig. 10(b).

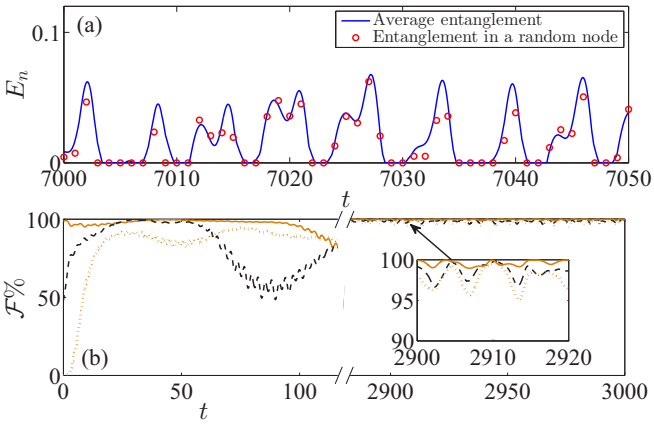

FIG. 10. (a) Entanglement measures of the quantum states in each cavity. (b) Initial state dependency of fidelity. Here the initial states of cavity fields are respectively selected as random coherent mix states. All the other parameters are the same as in Fig. 2.

VI. DISCUSSION

Here we give a brief discussion of the feasibility of quantum synchronization in a complex network, including the experimental feasibility of a coupled optomechanical array and the solvability of network synchronization conditions corresponding to Eq. (34). In our simulations, we select the same dimensionless parameters adopted in Mari's work, and they can meet the experimental requirements of most optomechanical systems. In a membrane (nano-object) optomechanical system especially, the parameter bounds are $\omega_m/(2\pi) = 134$ kHz, $m_{\rm eff} = 40 \sim 150$ ng, $\gamma = 4$ kHz, and $\kappa = 157$ kHz [65–68]. Correspondingly, $g \sim \gamma < \kappa$ is also a common coupling intensity in recent research into optomechanical systems [6,14,15,42,43]. In addition, phonon couplings between charged oscillators are also widely discussed in research on oscillator synchronization and optomechanical array [6,15].

In summary, we have proposed and analyzed a quantum state-sharing process in a complex quantum network. The quantum channel of this state-sharing process is based on quantum synchronized oscillators, and it will keep a strong quantum correlation in Markovian dissipation for a long time. In particular, we have discussed two typical complex networks to illustrate the effectiveness of our state-sharing process. An SW network can be regarded as independent communication between nodes in a network, and the state sharing occurs in linear motifs. Correspondingly, an SF network describes an information diffusion process, and all nodes need to be synchronized simultaneously in the network. By analyzing quantum synchronization, we find that linked nodes can directly achieve synchronization in an SW network, but the whole network can be synchronized only if the nodes are locally regulated to satisfy given synchronization conditions. In this case, $\mathcal{F} \to 100\%$ can be achieved in both SW and SF networks, and basically it is not influenced by the environment. For an SW network, a node can connect (disconnect) other nodes at any time without affecting the other links; for an SF network, external nodes can join the network at any time to obtain the same quantum state. These two properties ensure that our scheme is effective for QIP in complex network. Furthermore, we have also given a brief discussion of the experimental feasibility of our scheme.

We think some open aspects are worth being further investigated. For example, an unknown synchronous quantum state can be used to encrypt quantum states in the quantum state transfer process. Moreover, transmission of a continuous variable signal in a synchronized optomechanical system was discussed in Ref. [15]. Because the synchronization and state sharing are both effective in SW and SF networks, we think the scheme for quantum synchronization and state sharing discussed in our work can exhibit potential application values in communication networks.

ACKNOWLEDGMENTS

We thank Dr. J. Cheng, Dr. W. Z. Zhang, and Dr. Y. Zhang for the useful discussions. This research was supported by the National Natural Science Foundation of China (Grants No. 11574041 and No. 11175033).

APPENDIX A: DEDUCTION OF QUANTUM LANGEVIN EQUATIONS AND INPUT OPERATORS IN THE HEISENBERG PICTURE

In this Appendix, we will give the details of the deduction of quantum Langevin equations and input operators. We consider the point-to-point system coupling to an optical environment and an oscillator environment respectively. Similarly to previous works, the quantum environments are regarded as Boson thermal reservoirs, and the reservoirs are further assumed to consist of many oscillators with closely spaced frequencies and annihilation (creation) operators. Then the Hamiltonian of the system can be expressed as $H_{\rm total} = H + \sum_j (H_{Ej} + H_{Ij})$, where H is the system Hamiltonian corresponding to Eq. (11), and

$$H_{Ej} = \int_{-\infty}^{\infty} (\omega_{cj} - \omega_{lj}) c_j^\dagger(\omega_{cj}) c_j(\omega_{cj})\, d\omega_{cj} + \int_{-\infty}^{\infty} (\omega_{bj} - \omega_{mj})\, d_j^\dagger(\omega_{bj})\, d_j(\omega_{bj})\, d\omega_{bj} \tag{A1}$$

and

$$H_{Ij} = i \int_{-\infty}^{\infty} d\omega_{cj}\, g(\omega_{cj}) [a_j^\dagger c_j(\omega_{cj}) - a_j c_j^\dagger(\omega_{cj})] + i \int_{-\infty}^{\infty} d\omega_{bj}\, g(\omega_{bj}) [b_j^\dagger d_j(\omega_{bj}) - b_j d_j^\dagger(\omega_{bj})] \tag{A2}$$

are, respectively, the energies of the quantum environments (reservoirs) and the coupling between the quantum system and quantum environment with a rotating-wave approximation. The operators in the above expressions satisfy the following relations:

$$\begin{aligned} &[c_j(\omega_{cj}), c_j^\dagger(\omega'_{cj})] = \delta(\omega_{cj} - \omega'_{cj}), \quad [d_j(\omega_{bj}), d_j^\dagger(\omega'_{bj})] = \delta(\omega_{bj} - \omega'_{bj}), \\ &\langle c_j^\dagger(\omega_{cj}) c_j(\omega'_{cj}) \rangle = 0, \quad \langle d_j^\dagger(\omega_{bj}) d_j(\omega'_{bj}) \rangle = n_b(\omega_{bj}) \delta(\omega_{bj} - \omega'_{bj}), \end{aligned} \tag{A3}$$

if the optical environment is set to zero temperature but the oscillator reservoirs have a finite temperature T. Here n_b is the thermal phonon number satisfying the Boltzmann distribution $n_b(\omega_{bj}) = [\exp(\hbar\omega_{bj}/k_b T) - 1]^{-1}$.

With the full Hamiltonian H, dynamics of the jth system can be obtained with the following Heisenberg equations in the Heisenberg picture:

$$\begin{aligned}
\dot{a}_j &= [i\Delta_j + ig(b_j^\dagger + b_j)]a_j + E - \int_{-\infty}^{\infty} d\omega_{cj}\, g(\omega_{cj}) c_j(\omega_{cj}),\\
\dot{b}_j &= \left\{-i\omega_{mj}\left[1 + \frac{C_j(t)}{2}\right]\right\} b_j + iga_j^\dagger a_j + i\mu b_{3-j} - i\frac{\omega_{mj}}{2} C_j(t) b_j^\dagger - \int_{-\infty}^{\infty} d\omega_{bj}\, g(\omega_{bj})\, d_j(\omega_{bj}),\\
\dot{c}_j(\omega_{cj}) &= -i(\omega_{cj} - \omega_{lj}) c(\omega_{cj}) + g(\omega_{cj}) a_j,\\
\dot{d}_j(\omega_{bj}) &= -i(\omega_{bj} - \omega_{mj}) d(\omega_{bj}) + g(\omega_{bj}) b_j.
\end{aligned} \tag{A4}$$

Solving the bath operators in Eq. (A4), we have

$$\begin{aligned}
c_j(\omega_{cj}, t) &= e^{-i(\omega_{cj} - \omega_{lj})(t - t_0)} c_j(\omega_{cj}, t_0) + g(\omega_{cj}) \int_{t_0}^{t} dt' e^{-i(\omega_{cj} - \omega_{lj})(t - t')} a_j(t'),\\
d_j(\omega_{bj}, t) &= e^{-i(\omega_{bj} - \omega_{mj})(t - t_0)} d_j(\omega_{bj}, t_0) + g(\omega_{bj}) \int_{t_0}^{t} dt' e^{-i(\omega_{bj} - \omega_{mj})(t - t')} b_j(t'),
\end{aligned} \tag{A5}$$

corresponding to an input process ($t > t_0$). Substituting these solutions into the system operators in Eq. (A4), we obtain

$$\begin{aligned}
\dot{a}_j &= [i\Delta_j + ig(b_j^\dagger + b_j)]a_j + E\\
&\quad - \int_{-\infty}^{\infty} d\omega_{cj}\, g(\omega_{cj}) e^{-i(\omega_{cj} - \omega_{lj})(t - t_0)} c_j(\omega_{cj}, t_0) - \int_{-\infty}^{\infty} d\omega_{cj}\, g(\omega_{cj})^2 \int_{t_0}^{t} dt' e^{-i(\omega_{cj} - \omega_{lj})(t - t')} a_j(t')
\end{aligned} \tag{A6}$$

and

$$\begin{aligned}
\dot{b}_j &= \left\{-i\omega_{mj}\left[1 + \frac{C_j(t)}{2}\right]\right\} b_j + iga_j^\dagger a_j + i\mu b_{3-j} - i\frac{\omega_{mj}}{2} C_j(t) b_j^\dagger\\
&\quad - \int_{-\infty}^{\infty} d\omega_{bj}\, g(\omega_{bj}) e^{-i(\omega_{bj} - \omega_{mj})(t - t_0)} d_j(\omega_{bj}, t_0) - \int_{-\infty}^{\infty} d\omega_{bj}\, g(\omega_{bj})^2 \int_{t_0}^{t} dt' e^{-i(\omega_{bj} - \omega_{mj})(t - t')} b_j(t').
\end{aligned} \tag{A7}$$

We first consider the optical parts. Here we assume that the coupling intensity between environment and system is a flat spectrum without frequency dependence. So $g(\omega_{cj})$ can be replaced as a constant, and it does not need to occur in the integrand. By denoting $g(\omega_{cj})^2 \equiv \kappa/\pi$, Eq. (A6) can be rewritten as

$$\dot{a}_j = [i\Delta_j + ig(b_j^\dagger + b_j)]a_j + E - \sqrt{\frac{\kappa}{\pi}} \int_{-\infty}^{\infty} d\omega_{cj} e^{-i(\omega_{cj} - \omega_{lj})(t - t_0)} c_j(\omega_{cj}, t_0) - 2\kappa \int_{t_0}^{t} dt' \delta(t - t') a_j(t'). \tag{A8}$$

by using the relation $\int_{-\infty}^{\infty} d\omega e^{-i\omega(t - t')} = 2\pi\delta(t - t')$. Notice that $\int_{t_0}^{t} f(t')\delta(t - t') = \frac{1}{2}\int_{t_0}^{t_1} f(t')\delta(t - t') = \frac{1}{2} f(t)$ for $t_0 < t < t_1$ and then Eq. (A8) can be further simplified as

$$\dot{a}_j = [-\kappa + i\Delta_j + ig(b_j^\dagger + b_j)]a_j + E + \sqrt{2\kappa} a_j^{in}, \tag{A9}$$

by defining the input operator

$$a_j^{in} = -\frac{1}{\sqrt{2\pi}} \int_{-\infty}^{\infty} d\omega_{cj} e^{-i(\omega_{cj} - \omega_{lj})(t - t_0)} c_j(\omega_{cj}, t_0). \tag{A10}$$

Similarly, we can also simplify Eq. (A7) as

$$\dot{b}_j = \left\{-\gamma - i\omega_{mj}\left[1 + \frac{C_j(t)}{2}\right]\right\} b_j + iga_j^\dagger a_j + i\mu b_{3-j} - i\frac{\omega_{mj}}{2} C_j(t) b_j^\dagger + \sqrt{2\gamma} b_j^{in}, \tag{A11}$$

and the corresponding input operator is

$$b_j^{in} = -\frac{1}{\sqrt{2\pi}} \int_{-\infty}^{\infty} d\omega_{mj} e^{-i(\omega_{bj} - \omega_{mj})(t - t_0)}\, d_j(\omega_{bj}, t_0). \tag{A12}$$

Substituting Eqs. (A10) and (A14) into Eq (A3), we can obtain

$$\begin{aligned}
&\left\langle a_j^{in,\dagger}(t) a_{j'}^{in}(t') \right\rangle = 0,\\
&\left\langle a_{j'}^{in}(t') a_j^{in,\dagger}(t) \right\rangle = \delta_{jj'}\delta(t - t'),\\
&\left\langle b_j^{in,\dagger}(t) b_{j'}^{in}(t') \right\rangle = \bar{n}_b(\omega_{mj})\delta_{jj'}\delta(t - t'),\\
&\left\langle b_{j'}^{in}(t') b_j^{in,\dagger}(t) \right\rangle = (\bar{n}_b(\omega_{mj}) + 1)\delta_{jj'}\delta(t - t'),
\end{aligned} \tag{A13}$$

and the thermal connection functions are

$$\left\langle a_j^{in,\dagger}(t)a_{j'}^{in}(t') + a_{j'}^{in}(t')a_j^{in,\dagger}(t)\right\rangle = \delta_{jj'}\delta(t-t'),$$
$$\left\langle b_j^{in,\dagger}(t)b_{j'}^{in}(t') + b_{j'}^{in}(t')b_j^{in,\dagger}(t)\right\rangle = (2\bar{n}_b(\omega_{mj})+1)\delta_{jj'}\delta(t-t'). \tag{A14}$$

Equations (A11) and (A9) are exactly the same as the quantum Langevin equations used in the main text and (A14) is the corresponding second correlation functions. Now let us reexamine the above derivations; the only approximation we adopted is regarding varied coupling coefficient as a constant, which results in that the noise operator can correspond to a white noise with correlation function $\delta(t-t')$. The delta function makes integral-differential Heisenberg equations lose their integral terms. In this case the dynamical properties of the system no longer depend on its past history from $t = t_0$ to t'. This process can be said to be *Markovian*, and the quantum environments under this approximation will not have the memory effect.

APPENDIX B: PARAMETERS IN QUANTUM LANGEVIN EQUATIONS

The concrete form of the coefficient matrix S in the main text is

$$S = \begin{pmatrix} -\kappa & -\Gamma_1 & 0 & 0 & -2g\mathrm{Im}[A_1] & 0 & 0 & 0 \\ \Gamma_1 & -\kappa & 0 & 0 & 2g\mathrm{Re}[A_1] & 0 & 0 & 0 \\ 0 & 0 & -\kappa & -\Gamma_2 & 0 & 0 & -2g\mathrm{Im}[A_2] & 0 \\ 0 & 0 & \Gamma_2 & -\kappa & 0 & 0 & 2g\mathrm{Re}[A_2] & 0 \\ 0 & 0 & 0 & 0 & -\gamma & \omega_{m1} & 0 & -\mu \\ 2g\mathrm{Re}[A_1] & 2g\mathrm{Im}[A_1] & 0 & 0 & -\omega_{m1}[1+C_j(t)] & -\gamma & \mu & 0 \\ 0 & 0 & 0 & 0 & 0 & -\mu & -\gamma & \omega_{m2} \\ 0 & 0 & 2g\mathrm{Re}[A_2] & 2g\mathrm{Im}[A_2] & \mu & 0 & -\omega_{m2}[1+C_j(t)] & -\gamma \end{pmatrix} \tag{B1}$$

which contains the information of the mean value. Here $\Gamma_j = \Delta_j + 2g\mathrm{Re}[B_j]$.

[1] C. Huygens, *OEuvres completes de Christiaan Huygens* (Martinus Nijhoff, The Hague, 1893).
[2] Y. Xu, H. Wang, Y. Li, and B. Pei, Commun. Nonlinear Sci. Num. Sim. **19**, 3735 (2014).
[3] X. Wu, H. Wang, and H. Lu, Nonlinear Anal.-Real World App. **13**, 1441 (2012).
[4] L. Lü, C. R. Li, G. Li, A. Sun, Z. Yan, T. T. Rong, and Y. Gao, Commun. Nonlinear Sci. Numer. Sim. **47**, 267 (2017).
[5] L. Lü, C. R. Li, L. S. Chen, and G. N. Zhao, Nonlinear Dyn. **86**, 655 (2016).
[6] A. Mari, A. Farace, N. Didier, V. Giovannetti, and R. Fazio, Phys. Rev. Lett. **111**, 103605 (2013).
[7] V. Ameri, M. Eghbali-Arani, A. Mari, A. Farace, F. Kheirandish, V. Giovannetti, and R. Fazio, Phys. Rev. A **91**, 012301 (2015).
[8] M. H. Xu, D. A. Tieri, E. C. Fine, J. K. Thompson, and M. J. Holland, Phys. Rev. Lett. **113**, 154101 (2014).
[9] M. R. Hush, W. Li, S. Genway, I. Lesanovsky, and A. D. Armour, Phys. Rev. A **91**, 061401(R) (2015).
[10] T. E. Lee and H. R. Sadeghpour, Phys. Rev. Lett. **111**, 234101 (2013).
[11] T. E. Lee, C. K. Chan, and S. Wang, Phys. Rev. E **89**, 022913 (2014).
[12] S. Walter, A. Nunnenkamp, and C. Bruder, Phys. Rev. Lett. **112**, 094102 (2014).
[13] Y. Gul, arXiv:1412.8497v2.
[14] L. Ying, Y. C. Lai, and C. Grebogi, Phys. Rev. A **90**, 053810 (2014).
[15] G. Heinrich, M. Ludwig, J. Qian, B. Kubala, and F. Marquardt, Phys. Rev. Lett. **107**, 043603 (2011).
[16] W. Li, C. Li, and H. Song, Phys. Lett. A **380**, 672 (2016).
[17] A. Tavakoli, A. Cabello, M. Żukowski, and M. Bourennane, Sci. Rep. **5**, 7982 (2015);
[18] W. Heisenberg, Z. Physik **43**, 172 (1927).
[19] A. Galindo and M. A. Martín-Delgado, Rev. Mod. Phys. **74**, 347 (2002).
[20] J. Zhang, Y. X. Liu, S. K. Özdemir, R. B. Wu, F. Gao, X. B. Wang, L. Yang, and F. Nori, Sci. Rep. **3**, 2211 (2013).
[21] C. L. Zhu, N. Yang, Y. X. Liu, F. Nori, and J. Zhang, Phys. Rev. A **92**, 042327 (2015).
[22] A. J. Ferris and D. Poulin, Phys. Rev. Lett. **113**, 030501 (2014).
[23] W. B. Yan, J. F. Huang, and H. Fan, Sci. Rep. **3**, 3555 (2013).
[24] W. Qin, C. Wang, Y. Cao, and G. L. Long, Phys. Rev. A **89**, 062314 (2014).
[25] M. Walschaers, J. Fernandez-de-Cossio Diaz, R. Mulet, and A. Buchleitner, Phys. Rev. Lett. **111**, 180601 (2013).
[26] N. Kulvelis, M. Dolgushev, and O. Mülken, Phys. Rev. Lett. **115**, 120602 (2015).
[27] C. Chudzicki and F. W. Strauch, Phys. Rev. Lett. **105**, 260501 (2010).
[28] P. Pei, F. Y. Zhang, C. Li, and H. S. Song, Phys. Rev. A **84**, 042339 (2011).
[29] G. Manzano, F. Galve, G. L. Giorgi, E. Hernández-García, and R. Zambrini, Sci. Rep. **3**, 1439 (2013).
[30] J. Nokkala, F. Galve, R. Zambrini, S. Maniscalco, and J. Piilo, arXiv:1507.04635v2.
[31] P. Massobrio, V. Pasquale, and S. Martinoia, Sci. Rep. **5**, 10578 (2015).
[32] G. Bianconi and C. Rahmede, Sci. Rep. **5**, 13979 (2015).
[33] C. P. Zhu and S. J. Xiong, Phys. Rev. B **62**, 14780 (2000).
[34] G. Li, W. Hu, G. Xiao, L. Deng, P. Tang, J. Pei, and L. Shi, New J. Phys. **18**, 013012 (2016).

[35] W. L. Li, C. Li, and H. S. Song, Phys. Rev. E **93**, 062221 (2016).
[36] A. Farace and V. Giovannetti, Phys. Rev. A **86**, 013820 (2012).
[37] Y. Li, L. A. Wu, and Z. D. Wang, Phys. Rev. A **83**, 043804 (2011).
[38] P. C. Ma, J. Q. Zhang, Y. Xiao, M. Feng, and Z. M. Zhang, Phys. Rev. A **90**, 043825 (2014).
[39] J. Q. Zhang, Y. Li, and M. Feng, J. Phys.: Condens. Matter **25**, 142201 (2013).
[40] X. Y. Lü, J. Q. Liao, L. Tian, and F. Nori, Phys. Rev. A **91**, 013834 (2015).
[41] J. Cheng, Y. Han, and L. Zhou, J. Phys. B **47**, 045501 (2015).
[42] F. Marquardt and S. M. Girvin, Physics **2**, 40 (2009).
[43] M. Aspelmeyer, T. J. Kippenberg, and F. Marquardt, Rev. Mod. Phys. **86**, 1391 (2014).
[44] E. Y. Wembe and P. Yamapi, Commun. Nonlinear Sci. Num. Sim. **14**, 1439 (2009).
[45] M. O. Scully and M. S. Zubairy, *Quantum Optics* (Cambridge University Press, Cambridge, 1997).
[46] L. Tian, Phys. Rev. Lett. **110**, 233602 (2013).
[47] H. Miao, S. Danilishin, T. Corbitt, and Y. Chen, Phys. Rev. Lett. **103**, 100402 (2009).
[48] K. Børkje, A. Nunnenkamp, and S. M. Girvin, Phys. Rev. Lett. **107**, 123601 (2011).
[49] C. Genes, A. Mari, D. Vitalii, and S. Tombesi, Adv. At. Mol. Opt. Phys. **57**, 33 (2009).
[50] C. W. Gardiner and P. Zoller, *Quantum Noise* (Springer, Berlin, 2000).
[51] V. Giovannetti and D. Vitali, Phys. Rev. A **63**, 023812 (2001).
[52] A. Mari and J. Eisert, Phys. Rev. Lett. **103**, 213603 (2009).
[53] G. L. Wang, L. Huang, Y. C. Lai, and C. Grebogi, Phys. Rev. Lett. **112**, 110406 (2014).
[54] Y. C. Liu, Y. F. Shen, Q. H. Gong, and Y. F. Xiao, Phys. Rev. A **89**, 053821 (2014).
[55] Y. D. Wang and A. A. Clerk, Phys. Rev. Lett. **110**, 253601 (2013).
[56] H. Scutaru, J. Phys. A: Math. Gen. **31**, 3659 (1998).
[57] A. Isar, Phys. Part. Nuclei Lett. **6**, 567 (2009).
[58] G. Adesso and F. Illuminati, Phys. Rev. A **72**, 032334 (2005).
[59] G. Adesso, A. Serafini, and F. Illuminati, Phys. Rev. A **70**, 022318 (2004).
[60] L. M. Pecora and T. L. Carroll, Phys. Rev. Lett. **80**, 2109 (1998).
[61] D. J. Watts and S. H. Strogatz, Nature (London) **393**, 440 (1998).
[62] M. Barahona and L. M. Pecora, Phys. Rev. Lett. **89**, 054101 (2002).
[63] S. Garnerone, P. Giorda, and P. Zanardi, New J. Phys. **14**, 013011 (2012).
[64] The classical coupling does not need special synchronization conditions since it is allowed to have high coupling intensity. In an SF network, we set G^c to be the same as in an SW network to show this universality.
[65] M. Eichenfield, R. Camacho, J. Chan, K. J. Vahala, and O. Painter, Nature (London) **459**, 550 (2009).
[66] J. D. Thompson, B. M. Zwickl, A. M. Jayich, F. Marquardt, S. M. Girvin, and J. G. E. Harris, Nature (London) **452**, 72 (2008).
[67] O. Arcizet, P. F. Cohadon, T. Briant, M. Pinard, A. Heidmann, J. M. Mackowski, C. Michel, L. Pinard, O. Français, and L. Rousseau, Phys. Rev. Lett. **97**, 133601 (2006).
[68] F. Marquardt, J. P. Chen, A. A. Clerk, and S. M. Girvin, Phys. Rev. Lett. **99**, 093902 (2007).